THE AMERICAN SOCIETY OF MECHANICAL ENGINEERS
345 E. 47th St., New York, N.Y. 10017

97-GT-401

INNER WORKINGS OF AERODYNAMIC SWEEP

By

A.R. Wadia, P.N. Szucs and D.W. Crall
GE Aircraft Engines,
Cincinnati,Ohio 45215

ABSTRACT

The recent trend in using aerodynamic sweep to improve the performance of transonic blading has been one of the more significant technological evolutions for compression components in turbomachinery. This paper reports on the experimental and analytical assessment of the pay-off derived from both aft and forward sweep technology with respect to aerodynamic performance and stability. The single stage experimental investigation includes two aft-swept rotors with varying degree and type of aerodynamic sweep and one swept forward rotor. On a back-to-back test basis, the results are compared with an unswept rotor with excellent performance and adequate stall margin. Although designed to satisfy identical design speed requirements as the unswept rotor, the experimental results reveal significant variations in efficiency and stall margin with the swept rotors. At design speed, all the swept rotors demonstrated a peak stage efficiency level that was equal to that of the unswept rotor. However, the forward-swept rotor achieved the highest rotor-alone peak efficiency. At the same time, the forward-swept rotor demonstrated a significant improvement in stall margin relative to the already satisfactory level achieved by the unswept rotor. Increasing the level of aft sweep adversely affected the stall margin. A three-dimensional viscous flow analysis was used to assist in the interpretation of the data. The reduced shock/boundary layer interaction, resulting from reduced axial flow diffusion and less accumulation of centrifuged blade surface boundary layer at the tip, was identified as the prime contributor to the enhanced performance with forward sweep. The impact of tip clearance on the performance and stability for one of the aft-swept rotors was also assessed.

NOMENCLATURE

D-Factor	=	Diffusion Factor
IMM	=	Radial Immersion (0=tip, 1=hub)
LE	=	Leading Edge
PR	=	Pressure Ratio on an Operating Line
PRS	=	Pressure Ratio at Stall
PS	=	Pressure Surface
SM	=	Stall Margin
SS	=	Suction Surface
TE	=	Trailing Edge
TLE	=	Leading Edge Thickness
TMAX	=	Maximum Thickness
W	=	Inlet Corrected Flow on an Operating Line
WS	=	Inlet Corrected Flow at Stall
Δ	=	Change in clearance or efficiency relative to Rotor 4

INTRODUCTION

Swept wing theory has been used extensively to delay drag rise due to shock formation on aircraft wings over the last fifty years. However, workable swept blading applications in compressive turbomachinery design has only recently come of age, the reason for the delay being structural difficulties and the inadequacy of the aerodynamic design codes.

A series of attempts were made to exploit the concept of aerodynamic sweep for compressor blading between 1950 and 1970 by Beatty, Savage, and Emmery (1954), Goodwin (1957), Smith and Yeh (1963) and Lewis and Hill (1971). All these efforts were strictly analytical or confined to very low speed compressor testing with blades that contained linearly aft-swept leading edges. During the same time period (1966–1968), internally within GE Aircraft Engines, two swept blades for a TF39 outer panel application, one with aft sweep and one with forward sweep, were designed to explore the impact of aerodynamic sweep on transonic blading. The leading edges were swept in a linear manner. The aft-swept blade was tested and showed no noticeable improvement in efficiency relative to the unswept TF39 fan rotor as reported by Gostelow and Smith (1968). The forward-swept rotor was not tested because of low confidence in the structural integrity of the blades.

In the mid-seventies, NASA sponsorship resulted in the design and testing of the QF-12 swept fan stage as reported by Bliss, Hayden, Murray and Schwaar (1976), Lucas, Woodard and MacKinnon (1978) and Hayden, Bliss, Murray, Chandiramani, Smullin and Schwaar (1978). The preferred direction of sweep selected for the NASA program was aft-sweep. The measured aerodynamic performance was disappointing as the fan rotor was unable to achieve the flow, pressure ratio and efficiency goals. However, some acoustic MPT (multiple pure tone) noise improvements were measured with the aft-swept fan but they were still below design expectations.

In 1986, as a continuation of an experimental program initiated in 1971 by the Compressor Aerodynamic Research Laboratory (CARL) at Wright Patterson Air Force Base (WPAFB), the Air Force designed and tested an aft-swept rotor (Rotor 6) to evaluate the effect of sweep on the performance of transonic low aspect ratio compressor blades. The results were reported by Puterbaugh, Copenhaver, Hah and Wennerstrom (1996). Some additional results have also been reported by Hah and Wennerstrom (1990).

While the aft-swept Rotor 6 showed significant improvement in peak efficiency relative to the baseline rotor (Law and Wadia, 1993), its peak efficiency at design speed occurred at stall and the stall line fell significantly below the stall limit of the baseline rotor. Differences in lev-

Presented at the International Gas Turbine & Aeroengine Congress & Exhibition
Orlando, Florida — June 2–June 5, 1997
This paper has been accepted for publication in the Transactions of the ASME
Discussion of it will be accepted at ASME Headquarters until September 30, 1997

els and trends of speed-flow and efficiency-flow characteristics noted with Rotor 6 relative to the results with the baseline rotor suggested that perhaps more than just effects due to aerodynamic sweep were being encountered here. In fact, an internal analysis of the swept design showed this rotor to have less trailing edge effective camber. This suspicion was confirmed by test results from Rotor 4 (Wadia and Copenhaver, 1996), an unswept rotor designed by GE Aircraft Engines under USAF contract to achieve the baseline rotor's mass flow and pressure ratio specification, but having smaller throat area. Rotor 4 attained a design speed peak efficiency level matching that of the aft-swept Rotor 6 without any penalty being incurred by the stall line.

About the same time that this data set was being disseminated to the gas turbine industry within the United States by the Air Force, two other independent sets of data on high-speed, low-aspect-ratio aft-swept rotors were also becoming available to the compressor design community.

The first design and test data set was published by Neubert, Hobbs and Weingold (1990) and Rabe, Hoying and Koff (1991) on the Navy funded NAFCOT program specifically aimed at quantifying the effects of aft-swept rotors on high pressure ratio transonic fan stages. The fan was designed to be shock free by sweeping the leading edges aft beyond the Mach cone angle. The rotor was to achieve the same pressure ratio of 2.20 as an unswept baseline rotor having an inlet tip relative Mach number of 1.60. The test results of Rabe, Hoying and Koff (1991) were disappointing, indicating no improvement in spanwise mass averaged efficiency with the aft-swept rotor yet demonstrating a significant reduction in the stall line relative to the unswept baseline rotor. The reduction in stall line implies that at a given mass flow, the stalling pressure ratio is lower.

The second set of data available only to the United States gas turbine establishments included the design and testing of two aft-swept blades; the first for GE Aircraft Engines Joint Technology Demonstrator Engine and the other for a high-tip-speed, high-pressure-ratio multistage compressor. Results from both these tests once again re-emphasized the notion that aft-sweep fnr rotors with high tip loadings has an adverse impact on stall margin.

Up to this point, application of aerodynamic sweep in transonic blading was done with the intent to achieve performance gains by reducing the bow and passage shock strengths. The aerodynamic sweep can be used effectively to reduce the losses through the weaker detached leading edge bow wave. However, from a one-dimensional perspective, it is the shock-boundary layer interaction phenomenon, the required static pressure rise and the streamwise passage area variation and not the level of aerodynamic sweep that sets the passage shock strength in transonic blading. This pre-occupation with trying to reduce the passage shock strength tended to omit from consideration the aerodynamic sweep benefits derivable from radial flow migration and boundary layer centrifugation. Mohammed and Prithviraj (1977) and later Yamaguchi, Tominaya, Hattori and Mitsuhashi (1991) experimentally demnnstrated this type of benefit with forward sweep in a very low speed environment.

Prompted by the results with the unswept Rotor 4, a shift of focus away from the passage shock strength reduction, with the consequent, persistent trend of losing stall capability with aerodynamic aft-sweep, the Air Force and GE Aircraft Engines mutually agreed to a cooperative research arrangement in 1988 to quantify the benefits of aerodynamic sweep through tests with three swept rotors, aerodynamically equivalent to Rotor 4. Most of this paper deals with the results and insights gained from these single stage tests. To the best of our knowledge, the results with forward sweep, reported in this paper, are unique in the open literature on transonic blading.

SINGLE STAGE ROTOR DESIGNS

The aforementioned unswept Rotor 4 configuration, having excellent aerodynamic performance and stability, was selected as the technology base to be improved on by employing aerodynamic sweep technology. The design and test results of Rotor 4 have been reported in great detail by Copenhaver, Hah and Puterbaugh (1993) and by Wadia and Copenhaver (1996).

In addition to keeping the tip speed, inlet corrected flow and pressure ratio requirements the same, the swept blading was designed to retain the passage area distribution qualities of Rotor 4 in terms of throat margin, start margin and effective camber (Wadia and Copenhaver, 1996) to ensure that the perceived performance changes with the new blading is a consequence of aerodynamic sweep only. As part of imparting aerodynamic sweep into the blading and due to the mechanical constraints in executing the various sweep configurations, the chords, hence solidity (with constant blade count), the airfoil section edge and maximum thicknesses together with the axial location of maximum thickness could not be held fixed. These differences were viewed as essential and their performance impact, favorable or adverse, was considered to be the direct consequence of the particular "sweep package."

An aerodynamic synthesis of Rotor 4 test data served as the basis fnr the vector diagrams used to design the blading for the swept rotors. The detailed design procedure was identical to that used to design the unswept rotors and is presented in the paper by Wadia and Law (1993). In addition, a three-dimensional inviscid code coupled with a simple boundary layer analysis, available at the time of the design of the swept rotors in the late eighties, was used extensively in the design of the three swept rotors. The stator inlet conditions were held constant with each sweep configuration so that no major adverse or beneficial impact occurred to the overall performance of the stage. Minor adjustments to the rotor exit radial total pressure profile were made, when required, to accomplish this.

Table 1 summarizes the salient geometric and aerodynamic features of the baseline unswept Rotor 4.

Table 1: Rotor 4 Key Design Parameters

Parameter	
Specific Flow	43.61 lbm/sec-ft^2
Corrected Tip Speed	1500 ft/sec
Stage Pressure Ratio	1.92
Inlet Corrected Flow	61.81 lb/sec
Measured Stage Efficiency	0.8764
Inlet Radius Ratio	0.312
Tip Diameter	17 in
Number of Rotors/Stators	20/37
Mean Aspect Ratio (Rotor/Stator)	1.32/1.26
Average Solidity (Rotor/Stator)	2.3/1.68

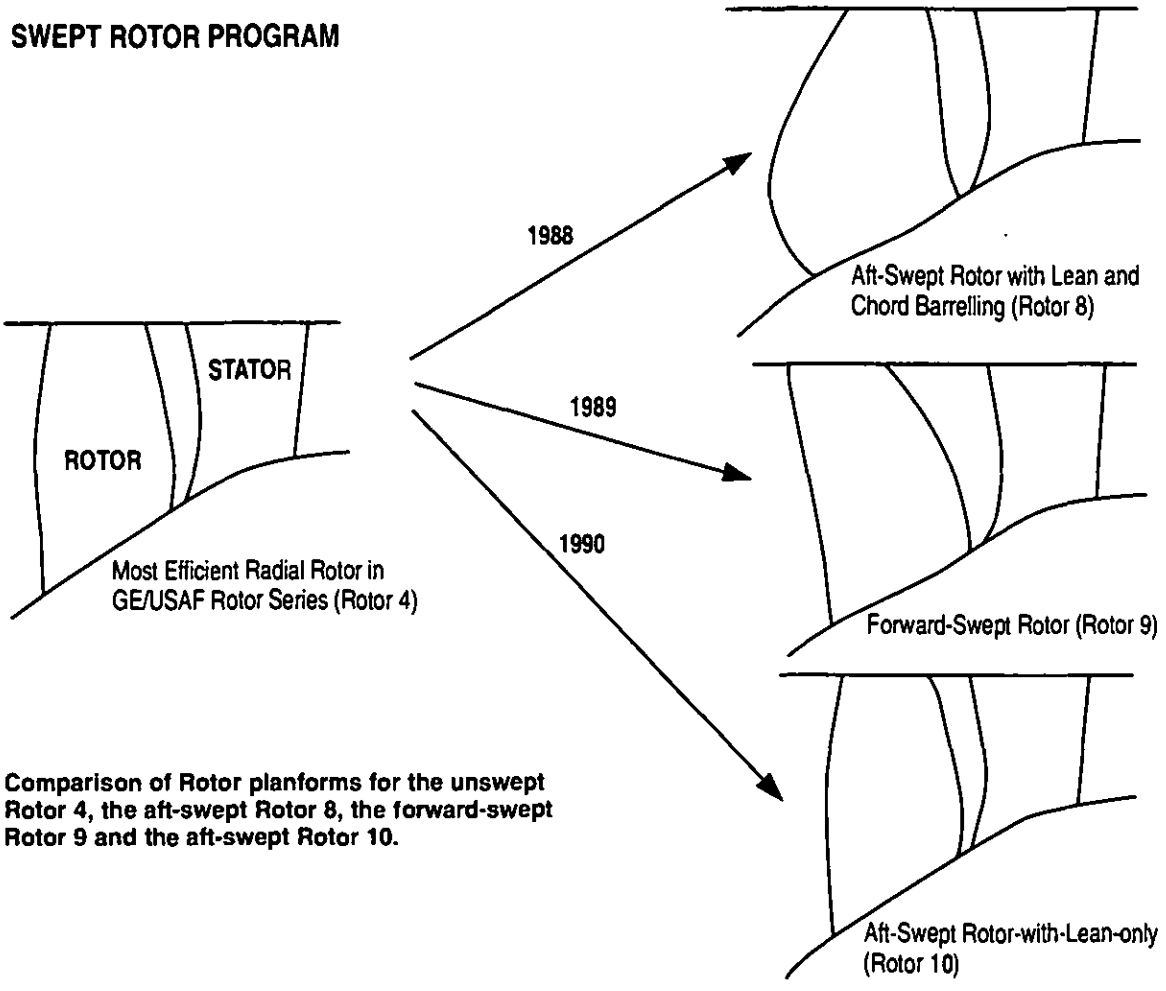

Figure 1. Comparison of Rotor planforms for the unswept Rotor 4, the aft-swept Rotor 8, the forward-swept Rotor 9 and the aft-swept Rotor 10.

Figure 1 compares the meridional views of the swept rotors relative to the unswept Rotor 4. The rotor inlet and exit hub and casing radii were retained such that on a one-dimensional basis the specific flow into the rotor and the following stator was constant among the configurations.

Rotor 8 was swept aft through a combination of barrelling the chord in the pitch region and leaning the blade tangentially opposite to the direction of rotation. Tangentially leaning the blade in the direction opposite to that of rotation imparts aft sweep to the rotor. Rotor 9 was swept forward using both chord barrelling and tangential lean in the direction of rotation. Sweeping the blades with chord barrelling increases both axial length and weight. To alleviate these two issues, and to assess sweep technology available for imbedded stages, another aft-swept blade, Rotor 10, was designed within the same planform as Rotor 4 imparting aft-sweep through tangential lean alone. The spanwise distribution of the normalized leading edge aerodynamic sweep is shown in Figure 2a. The leading edge aerodynamic sweep shown in Figure 2a was calculated using the method described by Smith and Yeh (1963) and further non-dimensionalized with the local value of the sweep at the tip of Rotor 4. Area ruled flowpath contouring to offset some of the metal blockage present was applied at the hub for all the rotors.

Figures 2b–2e compare the resulting solidity and normalized section thicknesses for the rotor blading. Rotor 10's geometrical parameters were similar to that for Rotor 4 and hence are not shown in these figures. Mechanically, as can be deduced from the section thickness plots in Figure 2, the swept blading presented differing design challenges. The swept forward Rotor 9 presented the most and the swept through lean only Rotor 10 the least. The two main issues with the swept forward configuration were that its lean increased the blade length, which required added root thickness to hold the flexural frequency, and its forward shifted tip sections required increased edge thicknesses to control the leading edge stresses. Conversely, sweeping aft with chord barrelling reduced the leading edge stresses. Although the trailing edge stresses increased, these were less of a concern from a FOD (Foreign Object Damage) point of view. For future product applications, development of the "Laser Shock Peening" process that reduces residual stresses in the leading edge or leading edge treatments such as protective coverings (Wadia, Crall, Prentice and Koch, 1996) could greatly reduce this disadvantage for forward-swept blading.

Table 2 presents the mechanical configuration comparison for the rotors. As a disadvantage, both the aft-swept Rotor 8 and the forward-

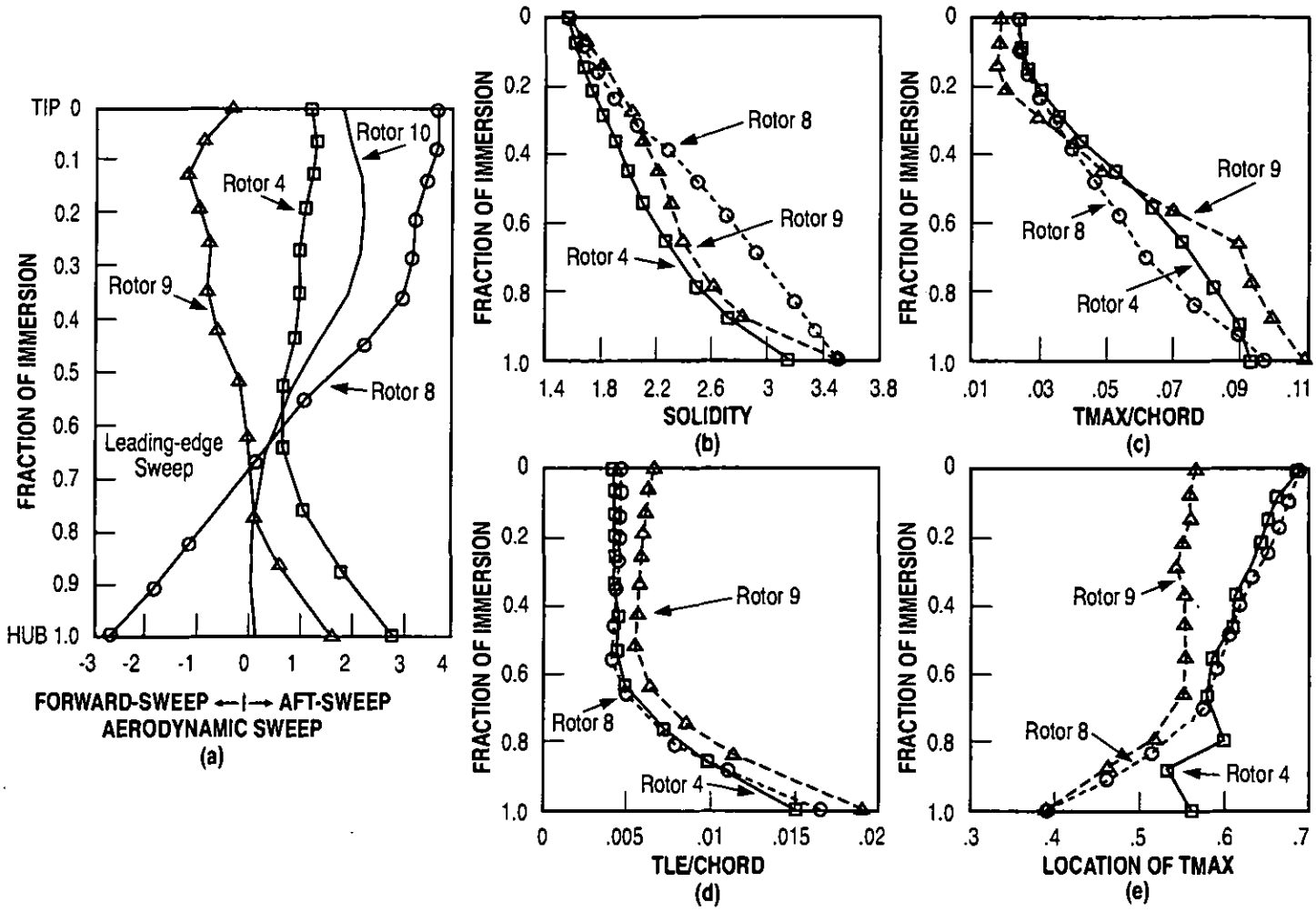

Figure 2. Comparison of the spanwise distribution of: (a) Non-dimensionalized leading-edge aerodynamic sweep, (b) Solidity, (c) Ratio of maximum thickness to chord, (d) Ratio of leading-edge thickness to chord, and (e) Fraction of location of maximum thickness from the leading edge.

swept Rotor 9 represented significant weight increases over the base unswept Rotor 4. While the aft sweep technology of Rotor 10 limited the achievable level of sweep, its weight and space impact was much less. A similar savings in weight and space would be available with a forward-swept version of Rotor 10. Although hollow blade technology is available to trade weight for expense, preliminary studies have shown the weight benefits from hollow construction are about the same for the radial and swept configurations, so the weight penalty for sweep would remain. Table 2 also shows that in addition to thickness increases, the forward-swept Rotor 9 required a material change to Ti17 that has superior mean stress capability and higher cost. Although beyond the scope of this paper, the information in Table 2 could be used to evaluate the DOC (Direct Operating Cost) of aerodynamic sweep technology by rating its performance impact against its weight and cost adder.

Table 2: Mechanical Design Parameter Summary

Parameter	Rotor 4	Rotor 8	Rotor 9	Rotor 10
Material	Ti6-4	Ti6-4	Ti17	Ti6-4
.2% Min Yield Strength (Ksi)	105	105	130	105
Weight (lbs/blade)	0.431	0.566	0.544	0.466
Tip Radial Growth (in)	0.012	0.020	0.015	0.013
Tip Chord (in)	4.05	4.05	4.05	4.05
Pitch Chord (in)	3.84	4.72	4.24	3.96
Hub Chord (in)	3.46	3.76	3.76	3.36

Another unique mechanical design feature observed with the forward-swept Rotor 9 was related to its "hot-to-cold" untwist characteristic, especially of the tip sections. While the unswept and the aft-swept rotors showed the airfoil tip sections twisting in the closed direction (conventional) as the rotational speed was reduced, the forward-swept Rotor 9 showed the tip sections twisting open as the speed was reduced. Simultaneously, as a consequence of this twist difference between the forward-swept rotor and the other rotors, the tip sections deflected axially aft as the rotational speed was increased with Rotor 9, while the deflection was axially forward in the case of the other rotors. These untwist differences have been documented by Wadia, Szucs, Niskode and Battle (1992).

TEST SETUP AND INSTRUMENTATION

The tests were conducted by the Air Force in the 2000-hp Compressor Aerodynamics Research Laboratory (CARL) at Wright Field. The single stage test vehicle has no inlet guide vanes and uses a cantilevered rotor to allow easy exchange of rotor designs with no impact on instrumentation. The rotors were of integral construction machined from single forgings.

Aerodynamics instrumentation consisted of 10 total temperature and 10 total pressure stator-exit radial rakes, each with 8 measurements at centers of equal area. The rakes were distributed around the circumference and spaced to divide a single vane exit passage into ten equal parts. Vane leading edge total pressure and total temperature instrumentation was also available and used to calculate the rotor-alone performance. Static pressure taps were located on the inner and outer endwalls at the inlet and exit plane of the stator. Dynamic pressure measurements and steady state static pressures along the casing over the blade tip were also acquired at key operating points. Inlet total pressure, total temperature, rotor speed and mass flow rate were also measured. All test data were acquired with some degree of depressed inlet pressure and later corrected to standard day inlet conditions as reported herein. Further details on the test setup, instrumentation and experimental precision error are described by Law and Wadia (1993).

The average measured (leading and trailing edge) running clearance for the baseline unswept Rotor 4 and the swept rotors is shown in Table 3. The forward-swept rotor's clearance is based on a single measurement at mid-chord.

Table 3: Average Rotor Clearance at Design Speed

Unswept Rotor 4	0.025 in
Aft-swept Rotor 8	0.030 in
Forward-swept Rotor 9	0.022 in
Aft-swept Rotor 10 (large clearance)	0.080 in
Aft-swept Rotor 10N (small clearance)	0.011 in

Aft-swept Rotor 10 data were obtained at two tip clearance levels and is presented later in the paper. Rotor 10 had the larger tip clearance and this rotor with the smaller tip clearance was designated as Rotor 10N. The correction in the stage efficiency at design speed due to the differences in tip clearance amongst the rotors was estimated using this data. The efficiency corrections (ΔEFFICIENCY, defined as the difference between the expected percent efficiency with Rotor 4's clearance and the percent measured test efficiency) are shown in Table 4.

Table 4: Efficiency Corrections for Clearance Variations at 100% Speed

ROTOR	ΔCLEARANCE	ΔEFFICIENCY
Rotor 4	0.000	0.00
Rotor 8	+0.005	+0.44
Rotor 9	-0.003	-0.26
Rotor 10N	-0.014	-1.22

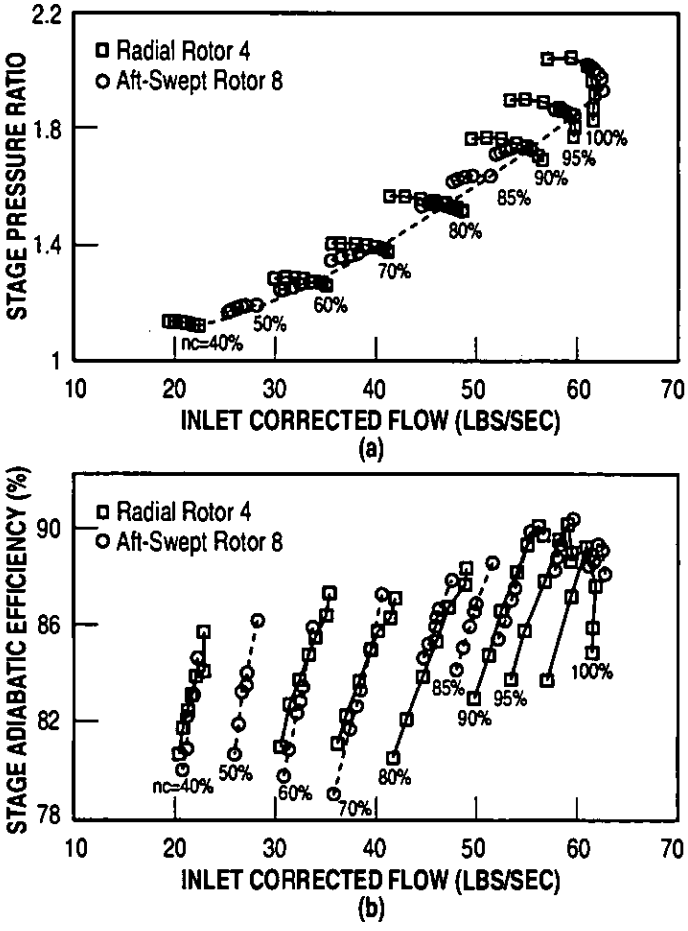

Figure 3. Comparison of measured stage performance for unswept Rotor 4 and aft-swept Rotor 8.

COMPARISON OF MEASURED STAGE PERFORMANCES

The overall performance of the swept rotors is compared with the performance of the unswept Rotor 4 in the following paragraphs. The efficiency and pressure ratio were determined through mass weighted averages of the measured exit pressures and temperatures. The most throttled-up data point for each speed shown on the compressor maps represents the last steady state data point acquired very near to where the stage stalled.

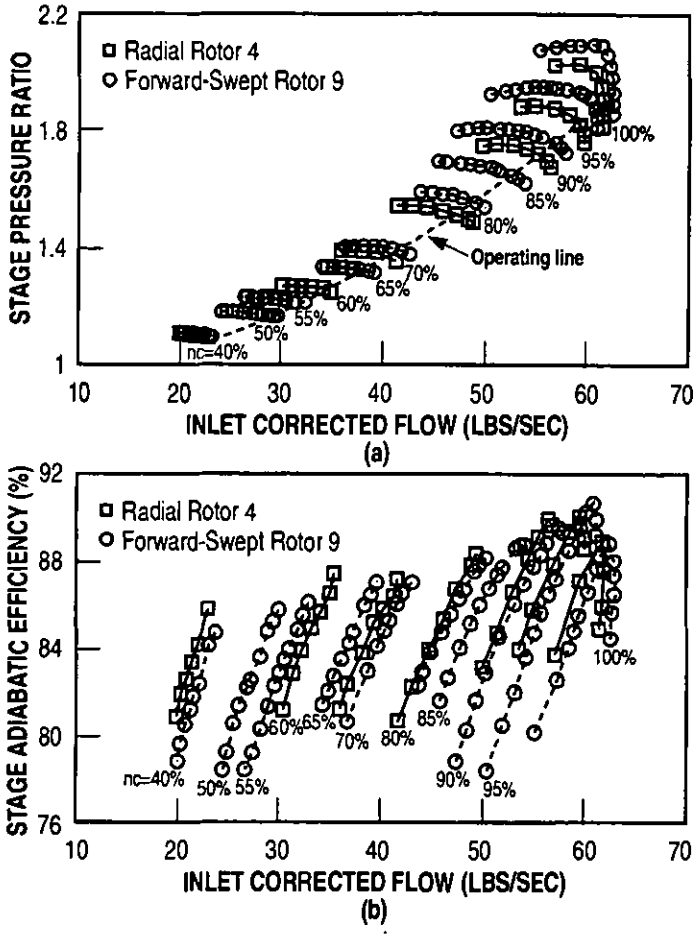

Figure 4. Comparison of measured stage performance for unswept Rotor 4 and forward-swept Rotor 9.

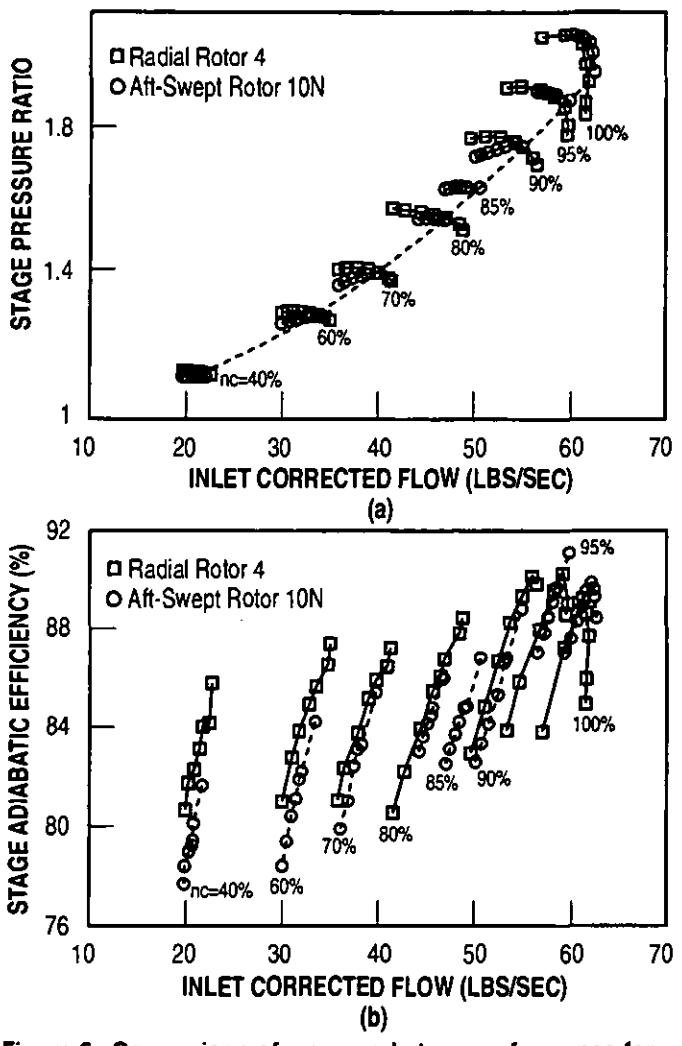

Figure 5. Comparison of measured stage performance for unswept Rotor 4 and aft-swept Rotor 10N.

Figure 3 shows the comparison of the measured stage performance of the aft-swept Rotor 8 and the unswept Rotor 4. The speed-flow trends along an operating line that passes through the design point are identical between both rotors except for the 1.8% increase in mass flow for Rotor 8 at design speed. This confirms the aerodynamic design equivalence between the two rotors. The peak efficiencies achieved by both rotors at design speed were approximately the same. The aft-swept Rotor 8 however shows an 8% reduction in the clean inlet stall line relative to Rotor 4.

The comparison of the measured stage performance between the forward-swept Rotor 9 and the unswept Rotor 4 is illustrated in Figure 4. Rotor 9 like Rotor 8 achieved about 1.5% higher mass flow rate at design speed. However, contrary to the trends at lower speeds observed with Rotor 8 (see Figure 3), the forward-swept rotor flowed significantly more than Rotor 4 along the nominal operating line. This improvement in the flow pumping with forward sweep could be attributed to a number of things, including its untwist characteristic (i.e., the airfoil sections twist open as the speed is reduced), lower effective specific flow (i.e., the blading is swept forward into a larger annulus area region) and reduced shock/boundary layer interaction losses in the blade outer panel. While the peak stage efficiencies at design speed were approximately the same for both rotors, the peak efficiency attained by Rotor 9 at 95% speed was 0.9 points higher relative to the unswept Rotor 4. Rotor 9 testing showed a significantly improved total pressure ratio characteristic when throttled, resulting in an 8% improvement in its stall line at constant flow relative to Rotor 4 at high speeds. Together with this flow pumping improvement at high speeds came significantly higher flow rollback.

At part speed (50 to 60% inlet corrected speed), a stall-flutter aeromechanical limit boundary was reached before the aerodynamic stall for Rotor 9. However, at these speeds the boundary was very near to the stall limit of Rotor 4. Also, relative to Rotor 4, at 70 and 80% speed, where Rotor 9 had no aeromechanical instabilities, the stall line remained unchanged with forward sweep. This was most likely due to Rotor 9's unconventional untwist which opens the airfoil sections at part speed. This structural untwist characteristic for Rotor 9 results in its shock being unstarted, forcing the tip leading edge incidences to higher levels at part speed.

Figure 5 shows the comparison of the measured stage performance for the aft-swept Rotor 10N (with the smaller clearance) and the unswept Rotor 4. Recall that this rotor has approximately half the level of leading edge sweep at the tip as Rotor 8. Similar to the other swept rotors the design flow achieved by Rotor 10N was approximately 1.8%

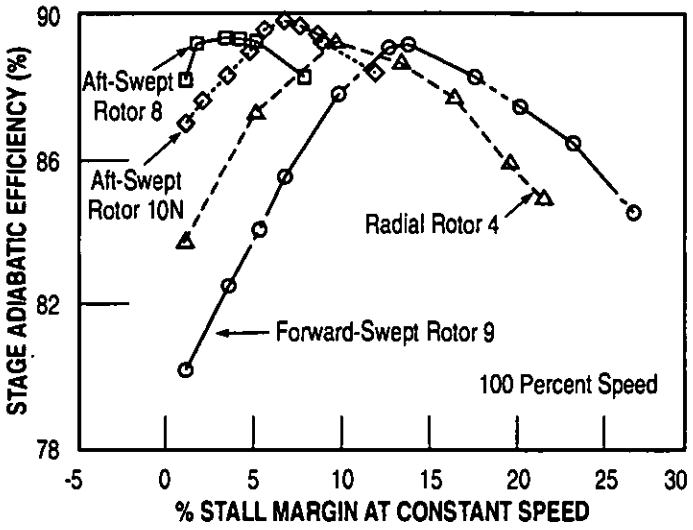

Figure 6. Comparison of the stage adiabatic efficiency versus stall margin for the baseline and swept rotors at design speed.

higher relative to Rotor 4, and the part speed mass flow pumping characteristic remained the same. The peak efficiencies for Rotor 10N were 0.8 and 1.0 points higher relative to Rotor 4 at 95 and 100% inlet corrected speeds, respectively. Consistent with other aft-swept rotor trends, the measured stall line was approximately 6% lower with the aft-swept Rotor 10N compared to Rotor 4's stall line.

The experimental data presented in Figures 3, 4 and 5, discussed above, suggests some possible minor improvement in stage efficiency with the aft-swept rotors but at a considerable loss in stall margin relative to the unswept Rotor 4. On the other hand, the forward-swept rotor, while basically retaining the stage efficiency, significantly increased the high speed stall line. Figure 6 shows the variation of the stage adiabatic efficiency with stall margin at design speed to further clarify the design implications of the data for practical applications with the swept rotors. The stall margin shown in Figure 6 was defined as:

$$SM = ((PRS/PR) \times (W/WS) - 1.0) \times 100\ \% \qquad (1)$$

where, each operating line point (for PR and W in eqn. (1)) is the corresponding steady state data point obtained along the 100% speed line. The peak efficiency for Rotors 4, 8, 10N and 9 occur at 9, 4, 7 and 13.5 percent stall margin, respectively. Generally, some (5–10%) stall margin is consumed by throttle transients, inlet distortion etc. in aircraft engine operation. The data in Figure 6 shows that peak efficiencies with aft-swept rotors occur too close to the stall line to be of practical use.

At part speed, the single stage test facility throttle opening (i.e., discharge valve fully open) limitations prevented attainment of the peak efficiency condition. As a result, no conclusive assessment of the preferred direction of sweep at low corrected speed conditions with regard to efficiency could be made.

COMPARISON OF MEASURED ROTOR PERFORMANCES

Further assessment of the performance of the rotors was obtained by calculating the adiabatic efficiency for the rotor only using

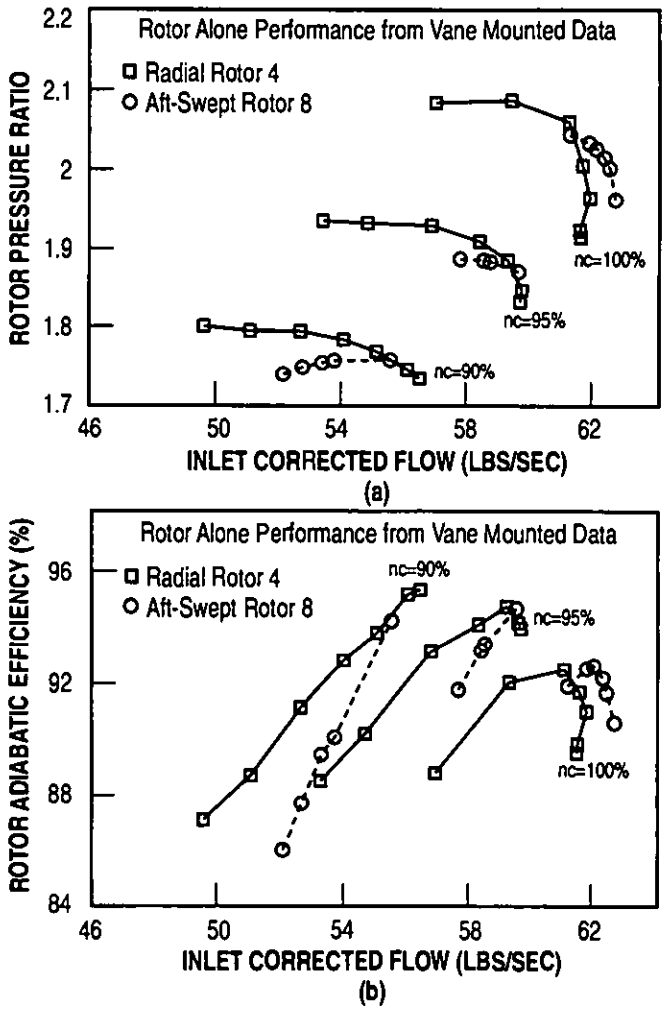

Figure 7. Comparison of Rotor (alone) performance (a) pressure ratio, (b) adiabatic efficiency; for the unswept Rotor 4 and aft-swept Rotor 8.

the measured stator leading edge values of total pressure and total temperature. The measured test data without any corrections for rotor tip clearance differences is presented in Figures 7 and 8 for Rotor 8 and Rotor 9, respectively. The correction in rotor-alone efficiencies due to the differences in tip clearance amongst the rotors would be similar to that shown in Table 4 for the stage efficiencies.

The peak rotor efficiencies for the aft-swept Rotor 8 and the unswept Rotor 4 are approximately equal as shown in Figure 7b. Similar trends in peak stage efficiency between the aft-swept and the unswept rotors were observed as shown in Figure 3b. However, the forward-swept Rotor 9 shows approximately 1 to 2 points improvement in peak rotor efficiency relative to Rotor 4 as shown in Figure 8b. The comparison of the peak stage efficiencies, shown in Figure 4b, shows this relative improvement to be less, suggesting that the stator losses could be higher with the forward-swept rotor. The larger gap between the rotor trailing edge and the stator leading edge, especially in the outer span, with the forward-swept rotor could be partly responsible for the higher stator losses.

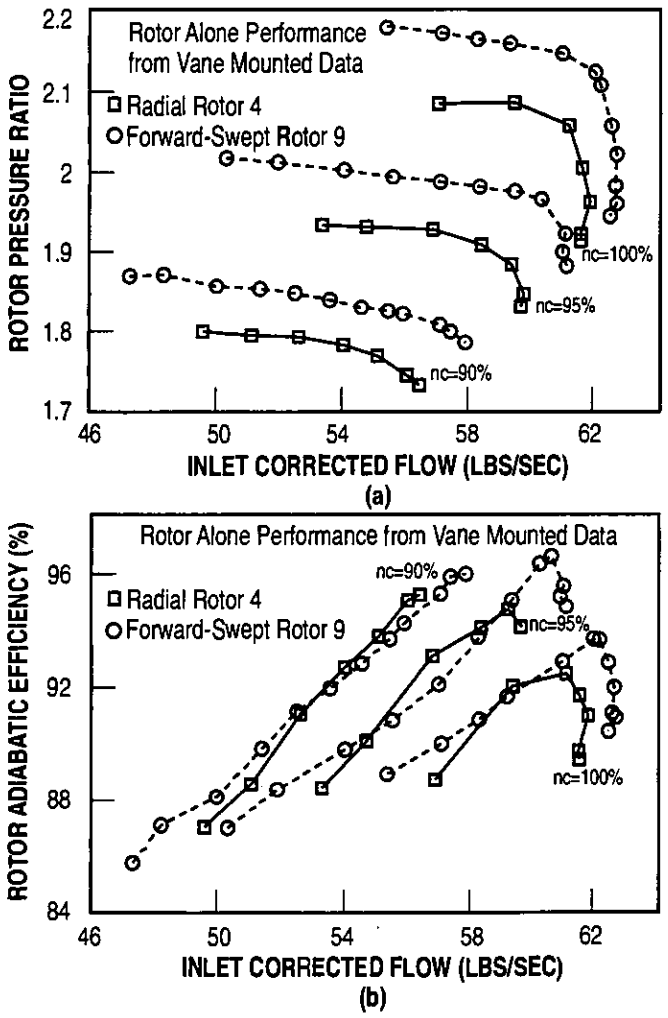

Figure 8. Comparison of Rotor (alone) performance (a) pressure ratio, (b) adiabatic efficiency; for the unswept Rotor 4 and forward-swept Rotor 9.

The test results presented so far with these aerodynamically equivalent swept rotors suggest a significant impact of aerodynamic sweep on the stall line with major rotor efficiency benefit with forward sweep. The efficiency benefit, however, is certainly not the several points in magnitude expected if the passage shock strength reduction proportional to the local aerodynamic sweep alone was the source of the improvement.

COMPARISON OF STAGE EXIT RADIAL PROFILES

Figure 9 shows the comparison of the spanwise distribution of the stage exit total pressure between the swept Rotor 8 and Rotor 9 and the unswept Rotor 4. The effects of throttling are included in each figure. All data have been corrected to standard day conditions.

The total pressure radial profiles for Rotor 4 show the normal behaviour with throttling in low radius ratio machines where the response at the tip is more than at the hub. In comparison, consistent with its lower stall line, the aft-swept Rotor 8's spanwise total pressure profile indicates a distinct weakness at the tip.

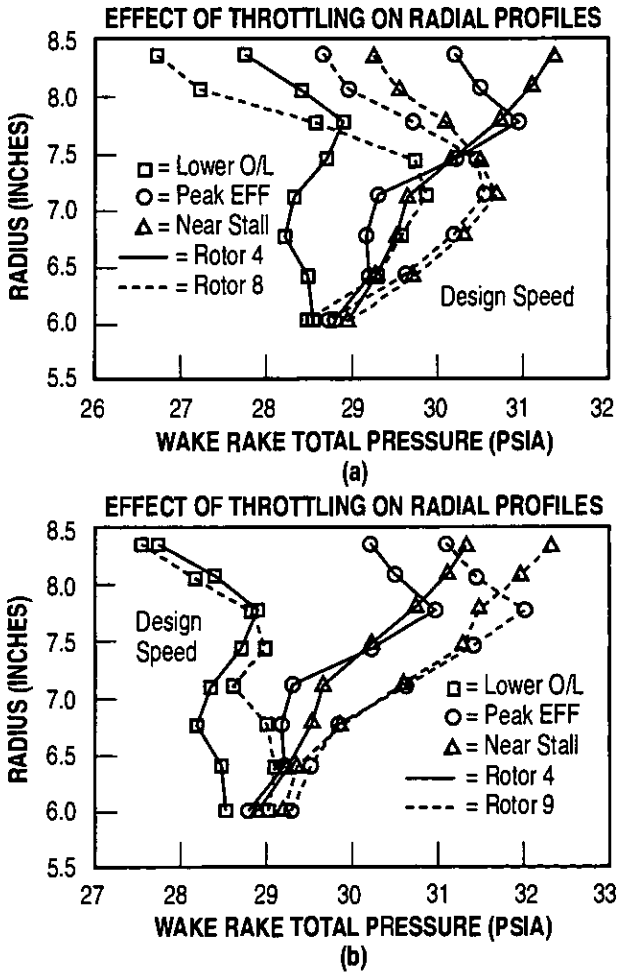

Figure 9: Comparison of the effect of throttling on the radial profiles of total pressure at design speed for (a) the unswept Rotor 4 and the aft-swept Rotor 8 and (b) the unswept Rotor 4 and forward-swept Rotor 9.

The measured efficiency profile comparison at the map peak efficiency condition at 95% speed is presented in Figure 10. There is an indicated improvement in efficiency near the tip with the forward-swept Rotor 9 and loss in efficiency with the aft-swept Rotor 8 relative to Rotor 4 in the tip region where the sweep is the largest. Ironically, the largest gain in efficiency with the aft-swept rotor is in the inner region where the chord flaring is the most, and the leading edge sweep is at or near zero. Again, the indication from this is that phenomena other than the conventional compressibility benefits that are customarily associated with aerodynamic sweep are at play here.

Although not shown, the radial profiles of both the total pressure and efficiency for Rotor 10N, the aft-swept rotor through lean only, showed trends very similar to that for Rotor 4.

DATA ANALYSES

The analytical results presented in this section are for the sole purpose of gaining an engineering understanding and interpretation of the test results regarding the inner workings of aerodynamic sweep and

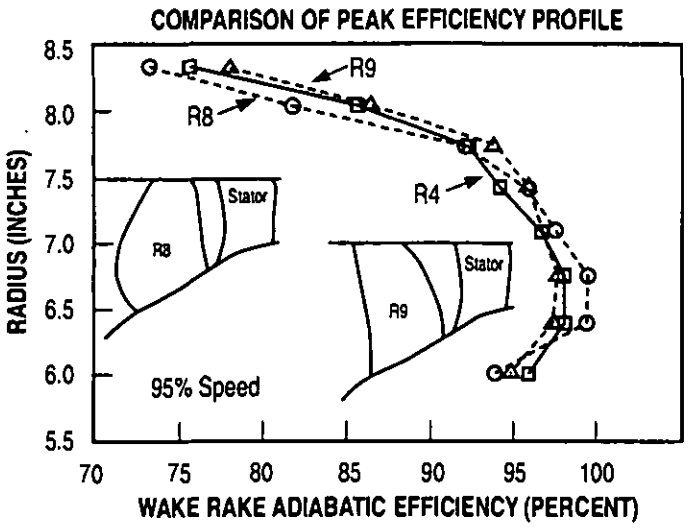

Figure 10. Comparison of the spanwise variation of adiabatic efficiency at 95% speed for Rotor 4, Rotor 8, and Rotor 9.

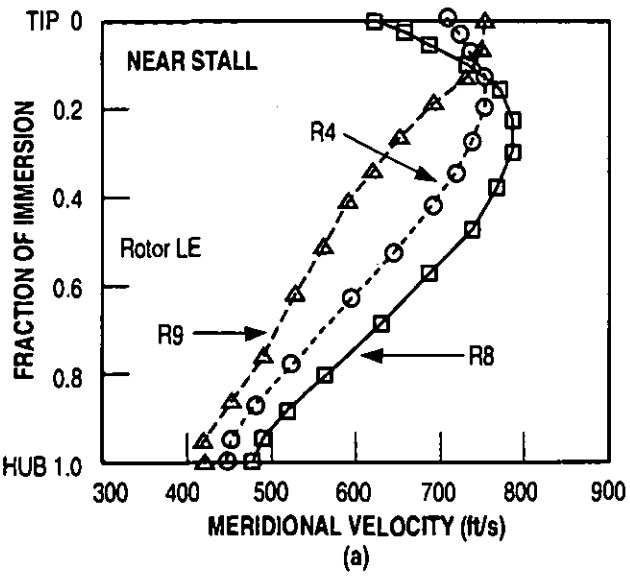

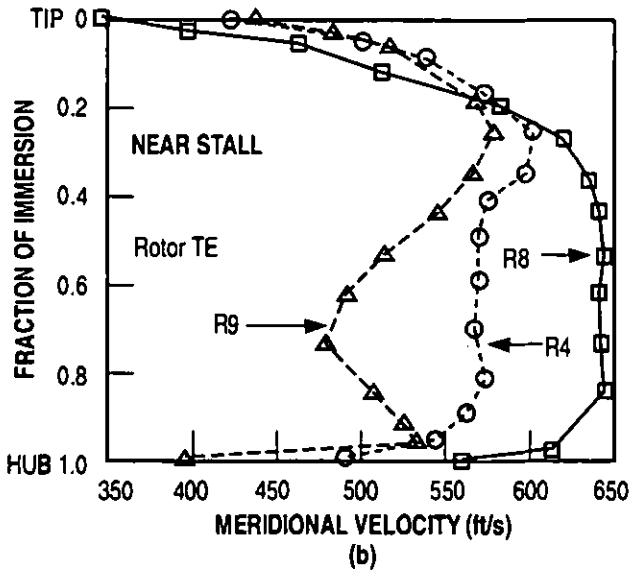

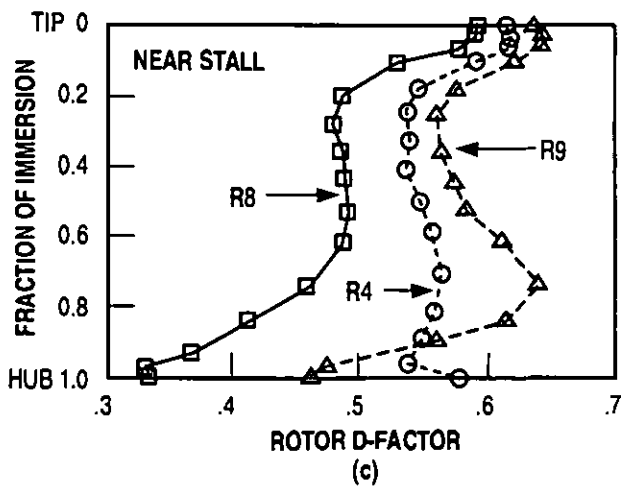

Figure 11. Comparison of the spanwise distribution of:
(a) Rotor leading-edge meridional velocity
(b) Rotor trailing-edge meridional velocity
(c) Rotor diffusion factor for Rotors 4, 8 and 9 at design speed near stall.

not for code validation purposes. While a much larger and more detailed body of work exists internally within GE Aircraft Engines, only selected supporting analytical results are presented in the paper. To streamline things further, the discussions in this section were limited to Rotors 4, 8 and 9 as representatives of the unswept, aft-swept and forward-swept aerodynamic technologies. In most cases, the observations noted concerning Rotor 8 also applied to Rotor 10N. In addition, more information is available regarding Rotor 10N's results in the paper by Copenhaver, Mayhew, Hah and Wadia (1996).

To gain insights into the aerodynamic loading characteristics of the rotors, datamatch results employing a two-dimensional axisymmetric throughflow analysis with models for secondary flow and mixing at design speed near the stall condition are presented in Figure 11. The comparisons of the spanwise distributions of the inlet and exit meridional velocities and the diffusion factor are illustrated in this figure. In interpreting these results, it must be remembered that the compressor map location of each of these near stall conditions are quite different in mass flow and attained pressure ratio. For example, the diffusion factor levels are significantly lower and the meridional velocity levels significantly higher relative to what is shown for Rotor 9 at the much lower throttle level (throttle level defined as pressure ratio/inlet corrected flow) that corresponds to the near stall condition for Rotor 8.

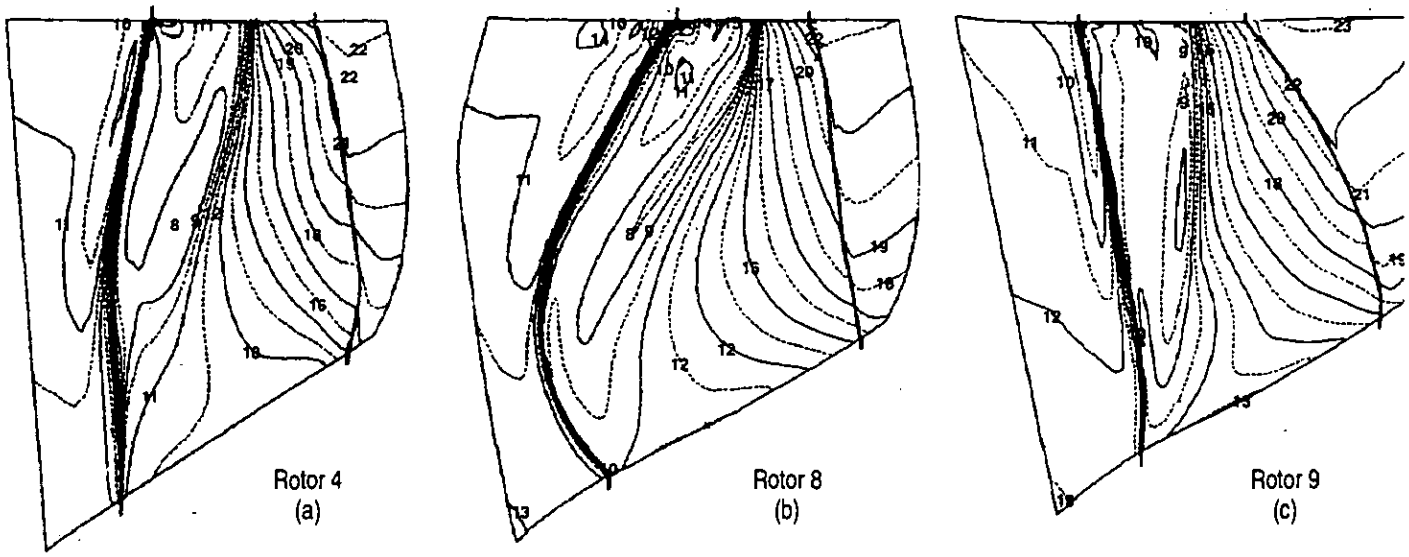

Figure 12. Comparison of the calculated contours of static pressure on the suction surface at design speed near peak efficiency for (a) Unswept Rotor 4, (b) Aft-swept Rotor 8, and (c) Forward-swept Rotor 9.

The spanwise distribution of the diffusion factor for Rotor 4 shown in Figure 11c indicates that aerodynamic loading wise the machine is tip limited, and is getting more so with aft sweep and less tip limited with forward sweep. As would be expected, the relative poorness in the measured stall lines is proportional to the magnitude of radial nonuniformity in the aerodynamic loading. The significantly more uniform loading distribution attained with the forward-swept blading (that is to say that the aerodynamic loading levels for the inboard sections are closer in level to the limiting tip value) allows this rotor to reach nearer its ultimate loading potential, while exactly the opposite is true with the aft-swept blading. The localized high loading level at the tip with Rotor 8 explains this rotor's tendency to reach a rotating stall type of stability limit (based on Kulite data), while the more balanced loading levels with Rotor 9 result in a surge type of stability limit at high speeds. The meridional velocities shown in Figures 11a and 11b also suggest more nonuniformity with the aft-swept rotor and less with the forward-swept blade. The aft-swept rotor pulls the flow away from the tip, while forward sweep tends to move the flow out toward the tip as originally observed in the low speed experiments of Mohammed and Prithviraj (1977). In addition to the increased meridional velocity non-uniformity with aft sweep, the meridional velocity diffusion from inlet to exit increases as well, contributing greatly to the earlier noted radial unbalance in the rotor diffusion factor.

Another adverse consequence of the large meridional velocity non-uniformity with the aft-swept rotor is the requirement on the resulting blade twist distribution. The rapid fall-off in meridional velocity toward the tip demands that a rapid twist closure toward the tip be implemented in the blading. As a result, the aft-swept rotor has very large acute dihedral angle (as defined in the paper by Smith and Yeh, 1963) at the tip along the suction side in the front half of the blading, while in contrast the forward-swept rotor with much less twist operates with near zero suction side dihedral angles at the tip. Acute dihedral angles are known to be adverse for endwall boundary layer flows, and this aspect is probably one of the major contributors to the poor aerodynamic stability and tip performance with aft-swept blading such as Rotor 8.

The throughflow analysis results at design speed, near stall were reported in the above paragraphs. After a similar throughflow analysis, the measured peak efficiency condition at design speed for the respective rotors was selected for further three-dimensional analysis to probe the internal flow quality differences and provide added insights into the inner workings of aerodynamic sweep. It is worth noting that as indicated in Figures 3 and 4, the corrected mass flow levels are identical for Rotors 8 and 9 at this condition. Also, in the case of Rotor 8 the peak efficiency condition is very near to its stall limit condition.

The details of the three-dimensional viscous code used, and which has found wide usage within General Electric Company for compressor and turbine design, has been reported by Turner and Jennions (1993). The inlet boundary conditions for the analysis consisted of uniform inlet total pressure and temperature and tangential flow velocity (zero in this case). The exit boundary condition consisted of prescribing a radial distribution of the circumferentially averaged static pressure determined by the throughflow analysis of the data at the stator inlet.

The three-dimensional analysis computed flows were 0.5 to 1.0 percent higher than those measured in the rig test for all the rotors analyzed. The agreement between the measured and calculated radial profiles of total pressure and temperature was good. The calculated axial distribution of the circumferentially averaged static pressure and the blade-to-blade contours of static pressure along the tip endwall were in good agreement with the static pressure and kulite data for all the rotors.

The resulting isobar contours on the suction surface for the three rotors are shown in Figure 12. The dense gradient in the isobars defines the shock intersections on the suction side, indicating a shock front that is nearly radial with the forward-swept Rotor 9 and slanted aft for Rotors 4 and 8. Although Rotor 4 is referred to as being unswept, its shock front indicates a small degree of inherent aft sweep resulting from its blade twist distribution. The most interesting isobar pattern results are with the highly swept Rotor 8. Contrary to the earlier reasoning regarding the influence of sweep on the passage shock strength from a one-dimensional viewpoint, Figure 12b illustrates a shock front for Rotor 8 that has been considerably diffused/eliminated in the blade's inner region, but

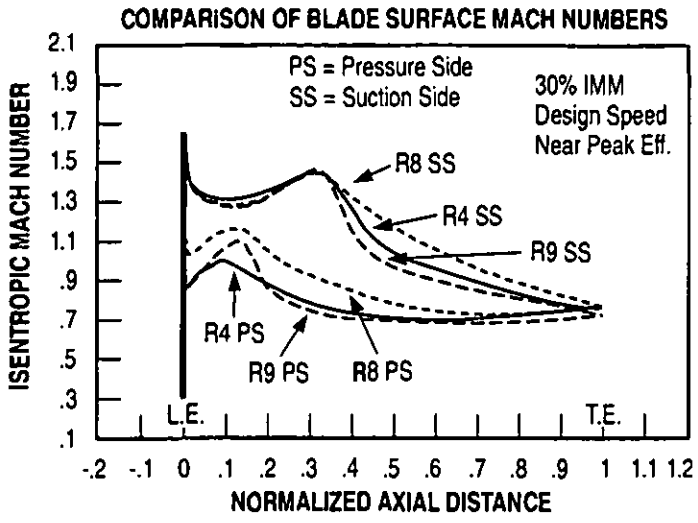

Figure 13. Comparison of rotor surface isentropic Mach number distribution at 30% immersion at design speed at peak efficiency.

then coalesces into a near normal strong shock front near the tip in agreement with the one-dimensional model described in the Introduction section. From a three-dimensional viewpoint, the highly skewed and considerably diffused shock front with Rotor 8 is attainable because of radial equilibrium considerations and the selection of proper blade chordwise camber distribution, aided in the case of Rotor 8 by the longer (barrelled) chords in the blade inner region. The assistance from radial equilibrium comes as a result of the skewed shock's downstream static pressure conditions in the blade's inner region being governed by the shock upstream region static pressures at the tip. These results support the radial trends in stage efficiency shown in Figure 10 that credited Rotor 8 with achieving the highest performance levels in the pitch region and below, and, consistent with its strong near normal shock front at the tip, had shown its tip performance level as the worst.

Added confirmation regarding Rotor 8's diffused shock front on the suction surface is provided in Figure 13. The surface isentropic Mach number distributions are compared among the three rotors at 30% immersion from the tip towards the hub. Compared to the suction side trends for Rotor 4 and 9, Rotor 8 indicates a shock free deceleration, albeit with a significantly high Mach number diffusion ratio (i.e., the ratio of the peak suction surface Mach number to the trailing edge Mach number) that the barrelled chords of Rotor 8 help or are perhaps required to tolerate without separation.

To get an insight to the boundary layer health and migration, Figure 14 compares the suction surface velocity vectors for the aft-swept Rotor 8 and the forward-swept Rotor 9 one grid off the airfoil surface representing a y+ of 10. Ironically, as shown in Figure 14a, the aft sweep of the blade leading edge combined with the radially increasing static pressure on the blade surface turns the flow into the shock front. The boundary layer health ahead of the shock appears to be good, as otherwise a radially outward pointing velocity vector indicative of centrifuged wake fluid would result. The same is indicated for the forward-swept rotor in Figure 14b.

However, when comparing the exit portion of the blading's suction surface velocity vectors, the results are significantly different between the two modes of aerodynamic sweep. Even behind the diffused

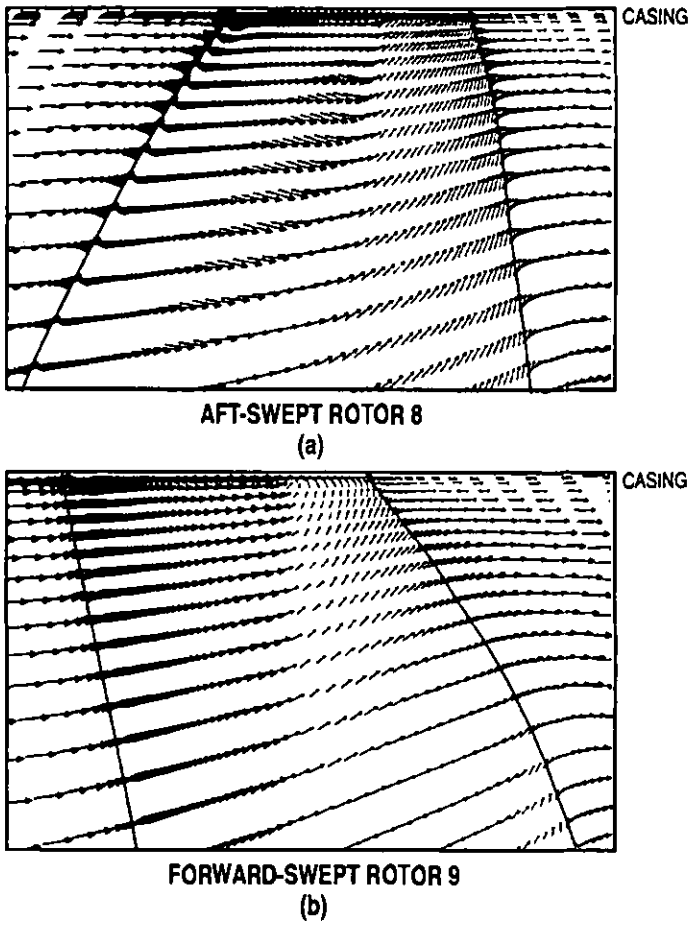

Figure 14: Comparison of the velocity vectors one grid line away (y^+=10) from the blade suction surface from pitchline to the casing at design speed near peak efficiency for (a) Rotor 8 and (b) Rotor 9.

portion of the shock front in Rotor 8, Figure 14a indicates a large deterioration/thickening of the boundary layer. The thickened boundary layer is shown to be centrifuged radially outward, adding in the outer region to the even more deteriorated conditions behind the strong portion of the suction side shock front, and then collecting at the outer casing. Due to this collection of low energy fluid at the tip, the weakened boundary layer cannot support the added diffusion that would be required of it had the shock front remained swept. Hence the shock front has to assume all of the required diffusion and it becomes normal.

With the forward-swept Rotor 9, Figure 14b shows a much healthier downstream boundary layer, even though its shock front, in the pitch region at least, is stronger relative to that of Rotor 8. It should be recalled, however, that in this region, according to Figure 10, Rotor 8's performance is superior to Rotor 9's. There is no indication of radially outward boundary layer centrifugation at all in the pitch region, and the centrifuged boundary layer accumulation at the tip appears to be much less relative to that with the aft-swept blading. It is also evident that with the swept-forward blading arrangement of shifting the tip sections forward, there is less tendency to collect the centrifuged boundary layer at the casing.

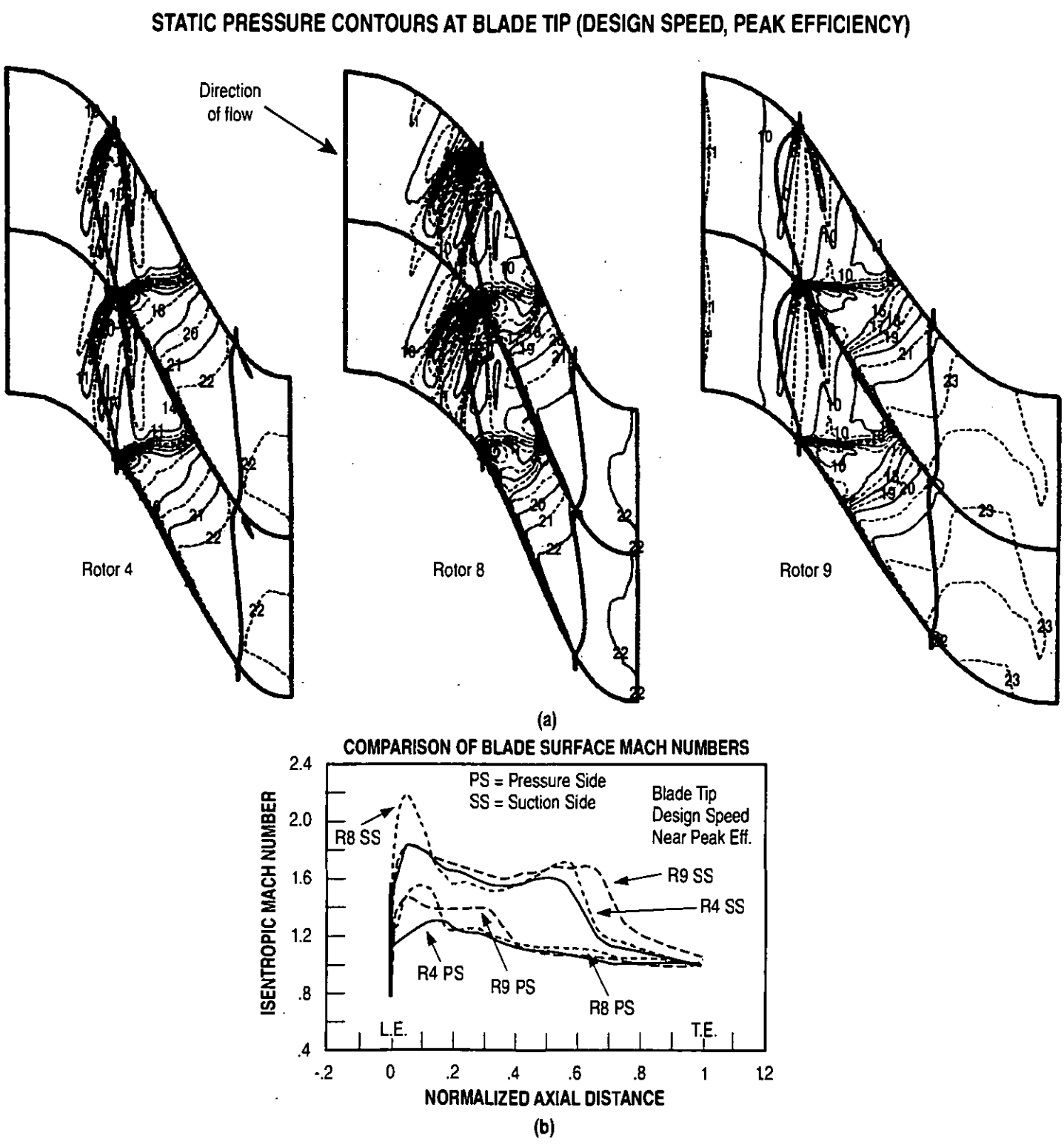

Figure 15. Comparison of the calculated (a) blade-to-blade contours of static pressure and (b) blade surface isentropic Mach number distribution at the blade tip at design speed near peak efficiency.

In the pitch region, the comparison of the trailing edge velocity vectors within the boundary layer indicating more wake fluid centrifugation with Rotor 8 as shown in Figure 14, suggests that from an aerodynamic stability viewpoint, for certain static pressure rise levels, it is preferable to achieve the static pressure rise through a combination of shock plus downstream diffusion rather than through shock free diffusion. Although the performance is indicated to be better with the latter, the added centrifuged wake fluid's contribution toward lower aerodynamic stability, as is the case with Rotor 8, might not make its use worthwhile.

The tip section blade-to-blade solutions and the surface isentropic Mach number distributions are compared in Figure 15. As expected, Rotor 9 looks best with a clean started inlet shock system resulting in a good incidence level. The aft-swept Rotor 8 is the worst, with the collected wake fluid blockage forcing an unstarted passage shock system that results in a high leading edge incidence level. The relative tip region performances indicated in Figure 10 are not hard to justify from Figure 15's results. Also, in addition to the collection of wake fluid at the casing with the aft-swept Rotor 8, the large acute dihedral angles along the suction side at the tip leading edge region is probably a major contributor to this rotor's endwall flow weakness causing its performance and aerodynamic woes at the tip.

EFFECT OF TIP CLEARANCE ON PERFORMANCE

The effect of tip clearance on the performance of transonic low aspect ratio rotors was investigated using the aft-swept Rotor 10 at two clearance levels shown in Table 3. Rotor 10 has the larger clearance with average clearance to blade height of 1.6 percent and average clearance to tip chord of 2 percent. Rotor 10N had the smaller clearance with an average clearance to blade height of 0.22 percent and average clearance to tip chord of 0.28 percent.

Figure 16 shows the comparison of the measured stage performance for the rotors at the two clearance levels. The average loss in design flow and stall margin with Rotor 10 was about 5.6 and 2.8 percent, respectively relative to Rotor 10N. The loss in design speed peak efficiency was about 6 points with the larger clearance rotor. The flow and efficiency derivatives with Rotor 10 for a given change in clearance over blade height is much larger than is usual with the more generally available conventional subsonic blading. This large reduction in efficiency is mainly attributed to the endwall shock/boundary interaction as shown by Copenhaver, Mayhew, Hah and Wadia (1996). But this strong, detached shock at the very tip of this blade may be an inescapable consequence of the aft sweep, and suggests that tip-weak, aft-swept blades may be inherently more sensitive to clearance variations.

Figure 17 shows the comparison of the spanwise distribution of the measured total pressure and stage efficiency for the two clearance levels at design speed and peak efficiency. The effect of the larger clearance is felt across the entire span and results in a significantly lower value of the total pressure at the tip. The reduction in efficiency is observed up to 65 percent immersion from the tip. While the "tip weak" exit profile of total pressure from the rotor also produced a slightly higher loss in the downstream stator, the increase in the rotor loss was the predominant driver in reducing the stage efficiency with the larger tip clearance.

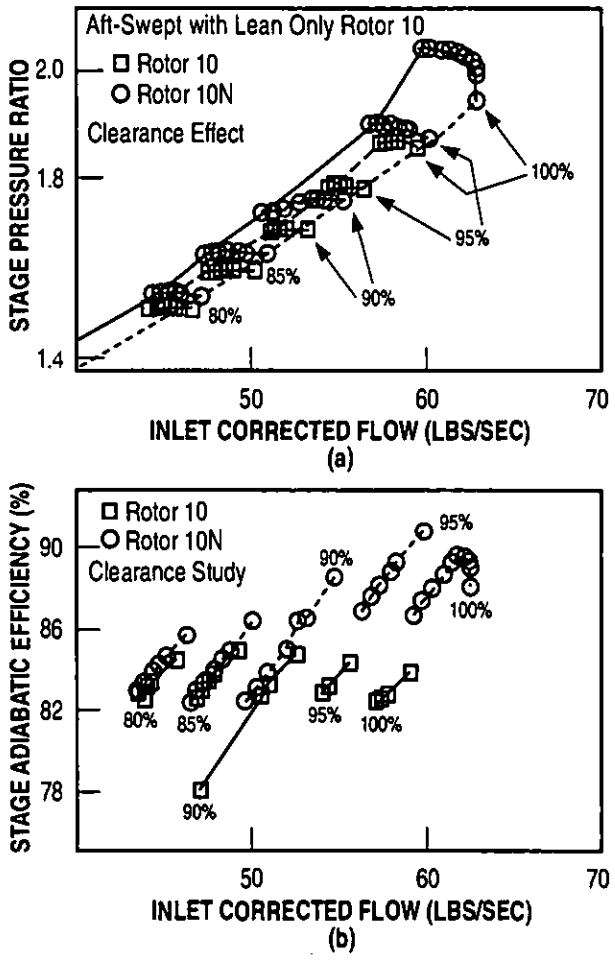

Figure 16. Comparison of measured stage performance for aft-swept Rotor 10 with small and large tip clearance.

CONCLUDING REMARKS

Both detailed experimental and analytical results of a study on the influence of sweep on transonic fan or compressor performance have been presented. The results for single stage applications are reported.

On an aerodynamic equivalent basis, the magnitude of stage performance improvement directly attributable to aerodynamic sweep was indicated to be upwards of one point in efficiency for the relative Mach number range of 1.5 to 1.6 investigated.

For the single-stage fans examined, the comparison of the measured performance shows that forward sweep can result in improvements in both efficiency and stall margin, a unique combination. The better performance of the forward-swept rotor, as explained with the support of three-dimensional viscous analysis, is attributed to the reduced shock/boundary layer interaction resulting from reduced axial flow diffusion, lower acute suction side dihedral angle in the leading edge and less accumulation of the blade surface boundary layer at the blade tip.

The penalty in the stall capability with aft-swept rotors, as determined in the single stage rig tests, appears to be a direct consequence of

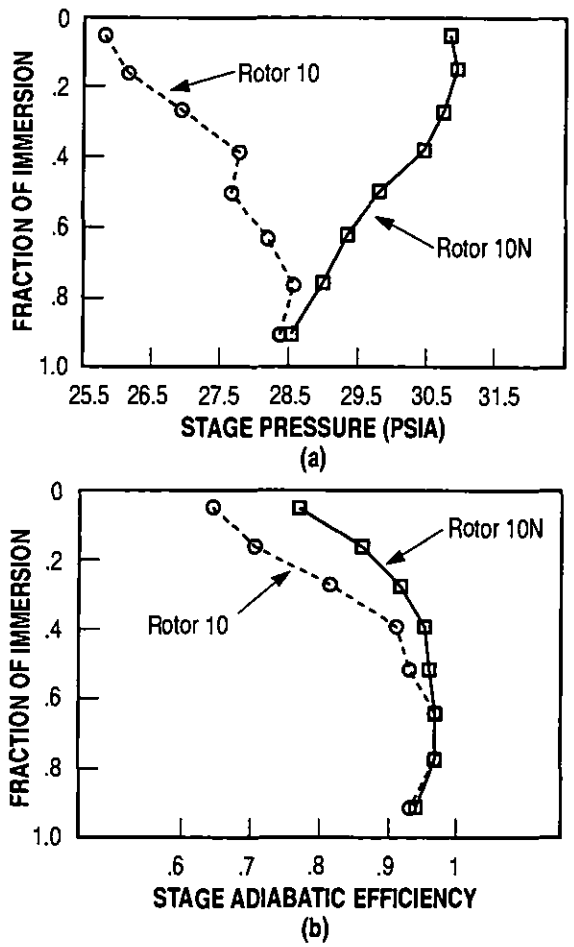

Figure 17. Comparison of spanwise variation of (a) stage pressure ratio (b) stage adiabatic efficiency for aft-swept Rotor 10 with small and large tip clearance at design speed at peak efficiency.

a locally high diffusion loading requirement at the tip being imposed on a weak endwall flow. The locally high loading requirement comes as a result of the aft sweep induced flow shift away from the tip, while the weak tip endwall flow results from the accumulation of the centrifuged suction side wake fluid and corner flows generated by the large acute suction side dihedral angles. While aft-swept blades achieve lower shock strength and better performance in the inboard sections, this comes at the expense of thickened trailing edge region boundary layers which are centrifuged and are likely to contribute to the aft-swept blades poor stall capability. In the case with forward sweep, however, the radial distribution in aerodynamic loading is much more uniform, and the endwall flow is much healthier due to less collection of wake fluid and the near zero tip suction side dihedral angles. All together, this results in the entire blade span performing nearer to the limiting loading capability at stall, and hence the superior stall line results at high speeds with forward sweep.

At part speed, the speed at which the blade reaches the shock "unstart" condition and below, no advantage in the aerodynamic stability limit is evident with either forward or aft-sweep. Also at part speed, the single stage test facility limitations prevented conclusive assessment of the preferred direction of sweep with regard to efficiency.

After assessing the impact associated with each direction of sweep in a single stage environment, the study was expanded to include the effects of forward sweep in a two stage fan where inlet distortion tolerance was also assessed. An investigation has been completed on a back-to-back basis using an unswept and a forward-swept stage 1 blade in the two stage configuration and the data will be reported at a later date. Some highlights of the results of this study obtained with the forward-swept rotor with inlet distortion has been reported by Kandebo (1996) and Ashley (1996).

The aerodynamic implications with aft and forward-swept blading have been explored in great detail on a back-to-back basis. The overall experimental results and the complementary three-dimensional viscous analyses suggest some unique improvements to efficiency and stall margin with forward-swept blading for tip loading limited transonic stages. Further studies are now underway to determine reduced-weight configurations that can utilize the advantages of forward-swept blading presented in this paper.

ACKNOWLEDGEMENTS

The authors would like to acknowledge the following individuals at Wright Patterson AFB for their excellent support in obtaining the data: Dr. Herb Law, Dr. Steve Puterbaugh, Dr. William Copenhaver, and Mr. Bob DeRose. We also thank Dr. Art Wennerstrom, Mr. John Lueke, Mr. Marvin Stibich of the USAF, and Pamela Battle. David Chang and Pat Niskode of GE for there support during the course of this investigation. We would also like to acknowledge Dr. Chunill Hah for performing all the pre-test 3D calculations at NASA and for providing us with an accurate assessment of the performance of the swept blades before the rig test. We are grateful to the management at GE and USAF for giving us permission to publish the single stage results of our investigation with swept blading.

REFFERENCES

Ashley, S., 1996, "Forward-swept Fan Moves Ahead," ASME Mechanical Engineering, Vol. 118, No. 1, pp. 142.

Beatty, L.A., Savage, M. and Emery, J.C., 1954, "Low Speed Cascade Tests of Two 45 Degree Swept Compressor Blades with Constant Spanwise Loading," NACA Research Memorandum, L53L07.

Bliss, D.B., Hayden, R.E., Murray, B.S., and Schwer, P.G., 1976, "Design Considerations for a Novel Low Source Noise Transonic Fan Stage," AIAA Paper No. 76-577.

Copenhaver, W.W., Hah, C., and Puterbaugh, S.L., 1993, "Three-Dimensional Flow Phenomena in a Transonic, High-Through-Flow, Axial-Flow Compressor Stage," ASME Journal of Turbomachinery, Vol. 115, pp. 240-248.

Copenhaver, W.W., Mayhew, E.R., Hah, C., and Wadia, A.R., 1996, "The Effect of Tip Clearance on a Swept Transonic Compressor Rotor," ASME Journal of Turbomachinery, Vol. 118, pp. 230-239.

Goodwin, W.R., 1957, "Effect of Sweep on Performance of Compressor Blade Sections as Indicated by Swept Blade Rotor, Unswept Blade Rotor and Cascade Tests, NACA TN 4062.

Gostelow, J.P., and Smith, L.H., 1968, "Aerodynamic Design and Performance of a Swept Back Rotor SW-1," GE Internal Report, 68-AEG-175.

Hah, C., and Wennerstrom, A.J., 1990, "Three-Dimensional Flowfields Inside a Transonic Compressor with Swept Blades," ASME Paper No. 90-GT-359.

Hayden, R.E., Bliss, D.B., Murray, B.S., Chandiramani, K.L., Smullin, J.I., and Schwaar, P.G., 1978, "Analysis and Design of a High Speed Low Noise Aircraft Fan Incorporating Swept Leading Edge Rotor and Stator Blades," NASA CR-135092.

Jennions, I.K. and Turner, M.G., 1993, "Three-Dimensional Navier Stokes Computations of Transonic Fan Flow Using an Explicit Flow Solver and an Implicit K-E Solver," ASME Journal of Turbomachinery, Vol. 115, pp. 261-272.

Kandebo, S., 1996, "General Electric Tests Forward-swept Fan Technology," Aviation Week and Space Technology, Sept. 23, pp. 32.

Law, C.H., and Wadia, A.R., 1993, "Low Aspect Ratio Transonic Rotors, Part I: Baseline Design and Performance," ASME Journal of Turbomachinery, Vol. 115, pp. 218-225.

Lewis, R.I., and Hill, J.M., 1971, "The Influence of Sweep and Dihedral in Turbomachinery Bladerows," Journal of Mechanical Engineering Science, Vol. 13, No.4.

Lucas, R.G., Woodard, R.P., and MacKinnon, M.J., 1978, "Acoustic Evaluation of a Novel Swept-Rotor Fan," AIAA Paper No. 78-1121.

Mohammed, K.P., and Prithviraj, D., 1977, "Investigation on Axial Flow Fan Impeller with Forward-swept Blades," ASME Paper No. 77-FE-1.

Neubert, R.J., Hobbs, D.E., and Weingold, H.D., 1990, "Application of Sweep to Improve the Efficiency of a Transonic Fan, Part -I Design," AIAA Paper No. 90-195.

Puterbaugh, S.L., Copenhaver, W.W., Hah, C., and Wennerstrom, A.J., 1996, "Investigation of an Aft-Swept Transonic Compressor Rotor," ASME Paper No. 96-GT-354.

Rabe, D., Hoying, D., and Koff, S., 1991, "Application of Sweep to Improve Efficiency of a Transonic Fan: Part II Performance and Laser Test Results," AIAA Paper No. 91-2540.

Smith, L.H., and Yeh, H., 1963, "Sweep and Dihedral Effect in Axial Flow Turbomachinery," ASME Journal of Basic Engineering, Vol. 85.

Wadia, A.R., Szucs, P.N., Niskode, P.N., Battle, P.M., 1992, "Forward-swept Rotor Blade," US Patent Number 5,167,489.

Wadia, A.R., and Law, C.H., 1993, "Low Aspect Ratio Transonic Rotors, Part 2: Influence of Location of Maximum Thickness on Transonic Compressor Performance," ASME Journal of Turbomachinery, Vol. 115, pp. 226-239.

Wadia, A.R., and Copenhaver, W.W., 1996, "An Investigation of the Effect of Cascade Area Ratios on Transonic Compressor Performance," ASME Journal of Turbomachinery, Vol 118.

Wadia, A.R., Crall, D.W., Prentice, I. and Koch, C.C., 1996, "Forward-swept Turbofan Blade with Non-Structural Leading Edge Extension," US Patent Filed, GE Aircraft Engines Patent Docket 13DV-12419.

Yamaguchi, N., Tominaga, T., Hattori, S., and Mitsuhashi, T., 1991, "Secondary-Loss Reduction by Forward-Skewing of Axial Compressor Rotor Blading," Presented at 1991 Yokohama International Gas Turbine Congress.